X-RAY SPECTROMETRY
X-Ray Spectrom. 2007; **36**: 150–157
Published online 2 April 2007 in Wiley InterScience
(www.interscience.wiley.com) DOI: 10.1002/xrs.955

Local structures in $Pb_{1-x}Mn_xTe$ systems†

I. Radisavljević,[1]* N. Ivanović,[1] N. Novaković,[1] N. Romčević,[2] M. Mitrić,[1] V. Andrić[1] and H.-E. Mahnke[3]

[1] Vinča Institute of Nuclear Sciences, P.O. Box 522. 11001 Belgrade, Serbia
[2] Institute of Physics, Pregrevica 118, Zemun, 11000 Belgrade, Serbia
[3] Bereich Strukturforschung, Hahn-Meitner-Institut Berlin GmbH, D-14109 Berlin, Germany

Received 21 December 2006; Accepted 9 January 2007

The semimagnetic semiconductor $Pb_{1-x}Mn_xTe$ is a good representative of IV-VI narrow-gap semiconductors, the class of materials in which phenomena like variation of the band gap with composition, negative magnetoresistance, long-term non-equilibrium processes, and the phonon dispersion anomalies, have been readily observed. The off-centering effects (i.e. displacement of the atoms from the regular lattice positions), and related low temperature ferroelectric phase transition, are also characteristic of these systems. In the attempt to resolve exact positions of both constitutive and impurity atoms, possibilities and features of their ordering and (or) clustering, and configurational and thermal disorder in the systems, we have performed EXAFS measurements at DESY-HASYLAB X1 and A1 beam lines, on Te and Mn absorption K-edges, for samples with different Mn concentrations (x = 0.002, 0.02, 0.1) at room temperature and 10 K. The results reveal that these systems are intrinsically quite disordered. The most significant deviations of the local structure from that predicted by X-ray diffraction measurements are found around Mn atoms, and increase with Mn concentration. Copyright © 2007 John Wiley & Sons, Ltd.

INTRODUCTION

The Pb–Te based compounds are narrow-gap semiconductors, with the band gap usually varying with the composition.[1] They can be used as infrared optoelectronic devices[2] and thermoelectric materials in two-dimension quantum well systems.[3] The effects of negative magneto resistance, long-term nonequilibrium processes,[1] and the phonon dispersion anomalies in the high symmetry phase have also been observed. In these materials electrically active native point defects (vacancies and interstitial atoms) produce energy states inside conduction and (or) valence band, leading to high charge carrier concentration in undoped crystals, on which neither cooling nor magnetic field produces the 'freeze-out' effect. The off-centering of atoms from the regular lattice sites, forming permanent dipoles and changing local conditions in the lattice, has been already registered in PbS_xTe_{1-x}, $Pb_{1-x}Sn_xTe_{1-y}Se_y$, $Pb_{1-x}Sn_xTe_{1-y}S_y$,[4–6] and $Pb_{1-x}Ge_xTe$.[7] In some of the cases, it is connected with the low temperature ferroelectric phase transition (FPT). In GeTe, SnTe and $Pb_{1-x}Sn_xTe$, FPT is related to the softening of the TO-mode at the Γ point of the Brillouin zone,[8] and in $Pb_{1-x}Ge_xTe$, to the ordering of dipoles formed by off-center ions.[9,10]

While PbTe has the NaCl structure (Fm-3m space group), with lattice constant 6.454 Å, MnTe has hexagonal NiAs structure ($P6_3/mmc$ space group), with lattice constants a = 4.078 Å, and c = 6.701 Å.[11] Thus appearance of a substantial strain in the PbTe lattice is expected upon introduction of Mn. Besides, $Pb_{1-x}Mn_xTe$ fulfils two major conditions for the phase transitions mentioned above. There is a large difference between Mn^{2+} and Pb^{2+} ionic radii of about 0.35 Å, and it is believed[12] that Mn^{2+} polarizability is about 1, much smaller than the polarizability of Pb^{2+} (4.82), which Mn^{2+} replaces in the crystal lattice. Yet, it is not quite clear in what way Mn is incorporated in the PbTe lattice. Although the $Pb_{1-x}Mn_xTe$ system has been investigated by different techniques,[13,14] extended X-Rays absorption fine structure (EXAFS) has proved to be a method of choice for studying local structures in multicomponent systems,[15–17] and has already provided some valuable contributions to off-centering and related phase transition investigations in similar systems.[4–7,10] Therefore, we have employed EXAFS to resolve the exact local structures around Te and Mn in $Pb_{1-x}Mn_xTe$ compounds, configurational and thermal disorder, and possible ordering and clustering of the Mn atoms. In addition, $Pb_{1-x}Mn_xTe$ is a suitable system for studying the frustration of the magnetic interactions in the fcc lattice. It undergoes spin–glass transition in the temperature range $0.07 < T_g < 4.2$ K (at least for concentrations $0.02 < \times < 0.2$).[13] The spin–glass properties are attributed to the long-range interband exchange interactions, enabled by a small E_g of these materials. Above T_g materials are in a superparamagnetic state. Some other questions, such as freezing of the Mn ions in the antiferomagnetic clusters are also opened. Obviously, introduction of Mn in PbTe leads to a strong modification of its band structure, which should be related to the mentioned structural modifications.

*Correspondence to: I. Radisavljević, Vinča Institute of Nuclear Sciences, P.O. Box 522. 611001 Belgrade, Serbia.
E-mail: iva@vin.bg.ac.yu
†Paper presented as part of a special issue of papers from the 2006 European X-ray Spectrometry Conference, Paris, France, 19–23 June. Part 3.

Copyright © 2007 John Wiley & Sons, Ltd.

SAMPLES, EXAFS MEASUREMENTS AND DATA PROCESSING

EXAFS measurements were performed on the uniformly doped $Pb_{1-x}Mn_xTe$ crystals with Mn concentrations of approximately $x = 0.002$, 0.02 and 0.1. Sample preparation and characterization as described in Ref. 14. Mn and Pb concentrations in the samples were checked by flame atomic absorption Spectrometry, using Perkin-Elmer 500 apparatus. The obtained results agree with the previously obtained[14] ones, in the limits of the measurements error. We also performed X-ray diffraction (XRD) measurements on the solid $Pb_{0.9}Mn_{0.1}Te$ sample using PHILIPS 1050 powder diffractometer with Ni filtered Cu $K_{\alpha 1,2}$ radiation (40 kV and 20 mA) and Bragg-Brentano focusing geometry. The pattern (Fig. 1) was taken in the $20^\circ \leq 2\theta \leq 90^\circ$ range with step of 0.05° and exposure time of 9 s per step. The obtained lattice parameter (6.4294 Å) is in good agreement with the one (6.433 Å) reported earlier.[14] According to the results presented in Fig. 1, the $Pb_{0.9}Mn_{0.1}Te$ sample is of the single NaCl phase. There is no evidence of other phases, except for the peak at $2\theta \approx 20^\circ$ (marked with the star in Fig. 1), which corresponds to a small amount of oxides, which are present in the PbTe systems.

The Tellurium K-edge EXAFS data were collected at beamline X1, and the Mn K-edge data at A1 beamline of HASYLAB at DESY. The synchrotron radiation source was operating at electron beam energy of 4.5 GeV with a maximum stored current of 200 mA. We used Si-(111) crystal monochromator on experimental station A1 for measurements at Mn K-edge and Si-(311) on experimental station X1 for measurements at Te K-edge. Samples were oriented at 45° to the incident beam and a seven segment Ge detector, supplied by HMI-Berlin, was used to collect spectra in the fluorescence mode. Multiple scans were taken to improve the signal-to-noise ratio. Data analyses were performed using IFEFFIT and related programs,[18–23] as implemented in the ATHENA and ARTEMIS packages.[24] The self-absorption attenuation of the amplitude of the spectra measured at the tellurium K-edge were taken into account for tellurium concentration and actual sample dimensions using the Booth and Bridges algorithm.[24]

The oscillatory part of the measured X-ray absorption coefficient $\mu(E)$, was background-corrected by a smooth background spline function $\mu_0(E)$ and normalized,[20] providing the EXAFS function:[25]

$$\chi(E) = \frac{\mu(E) - \mu_0(E)}{\Delta\mu}$$

The examples of the normalized experimental spectra (with the background determined (dashed line)) measured at room temperature (RT) at Te K-edge and Mn K-edge in Sample 3 ($Pb_{0.9}Mn_{0.1}Te$), are presented in Fig. 2(a) and (b) respectively. The extracted EXAFS function was converted from energy to photoelectron wave vector (k) space $\chi(k)$ and related to the equation:[25]

$$\chi(k) = \sum_j \frac{N_j}{kR_j^2} S_0^2(k) F_j(k) \cdot e^{-2k^2\sigma_j^2} \cdot e^{\frac{-2(R_j - \Delta)}{\lambda}} \cdot \sin[2kR_j + \delta_j(k)]$$

where N_j is the number of atoms in the jth shell; R_j-the mean distance between the absorbing atom and the j-th shell; $F_j(k)$-the magnitude of the backscattering amplitude of the j-th neighbor atom; $\delta_j(k)$-the electronic phase shift. Amplitude reduction factor, S_0^2, originally introduced to describe the central atom shake-up and shake-off effects, actually accounts for all amplitude corrections. The photoelectron

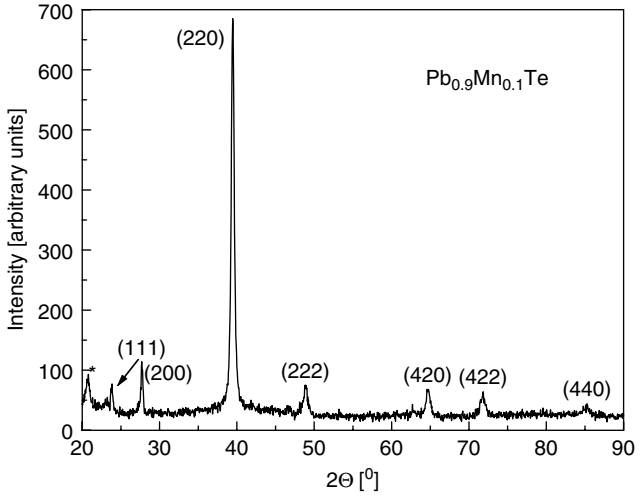

Figure 1. XRD spectra of the $Pb_{0.9}Mn_{0.1}Te$ sample.

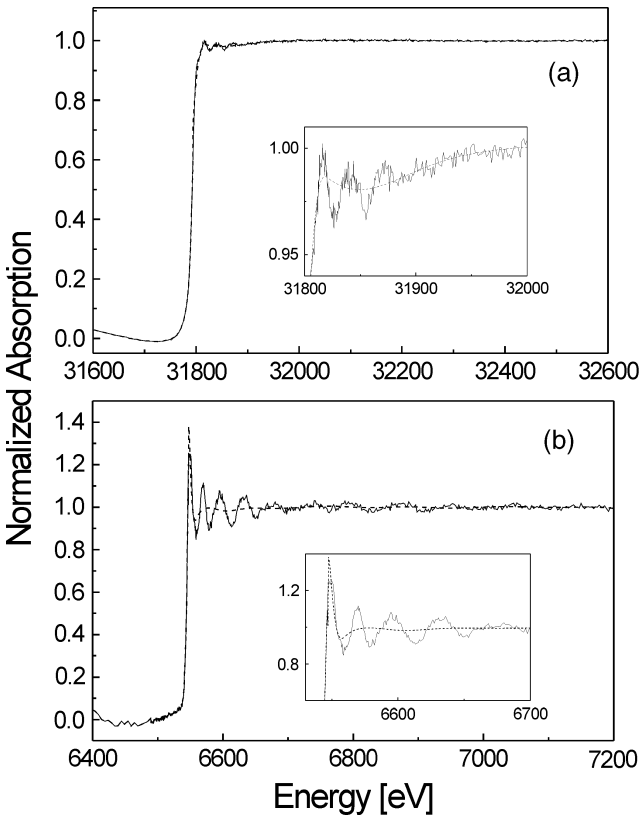

Figure 2. Normalized experimental EXAFS spectra with the background determined (dashed line) obtained at RT (a) Te K-edge (b) Mn K-edge of Sample 3 ($Pb_{0.9}Mn_{0.1}Te$).

Copyright © 2007 John Wiley & Sons, Ltd.

DOI: 10.1002/xrs

X-RAY Spectrometry

mean free path, λ, is the mean distance reached by the photoelectron without inelastic scattering. The decay of the EXAFS amplitude due to the mean free path or finite lifetime (including core-hole lifetime) of the photoelectron is captured by the exponential term $e^{-2(Ri-\Delta)/\lambda}$. The parameter $\Delta \approx R_j$, is a 'core radius' of the central atom and eliminates double counting of inelastic processes in the core region. σ_j^2 is the mean squared displacement between the absorbing atom and an atom in the j-the shell including both configurational and thermal disorder. Some characteristic $k\chi(k)$ spectra of the three measured samples are presented in Fig. 3.

Fourier transformation (FT) of the $k\chi(k)$ function was performed over the k range between k_{min} ranging from 2.0 to 3.0 Å^{-1} and k_{max} ranging from 8 to 12 Å^{-1} depending on the quality of the investigated spectra using the Hanning window. The k_{min} and k_{max} values were chosen at node points to minimize the spectral broadening. In order to minimize the unphysical Fourier peaks in the low FT region, R_{bkg} value of 1.5 was chosen. The FEFF8.2 code[19] was used to calculate theoretical phase and amplitude functions of the involved scattering paths, which were obtained from the atomic coordinates provided by ATOMS program.[21] FEFFIT program[22] is used to analyze the $\chi(k)$ data. Data were fitted allowing σ^2, R_j, N_j and the single edge shift correction (E_0), to be adjusted for each shell, unless reported otherwise. The fact that parameter E_0, which accounts for all phase shift corrections, might be element specific,[23] motivated us to allow for its different values for different shells, in some cases. According to FEFF 8.2 calculations, amplitudes of multiple scattering paths have negligible contribution, therefore the presented analyses involve only single scattering paths. For each sample, the value of S_0^2 was estimated by observing the $\sigma^2(S_0^2)$ dependence for $k\chi(k)$, $k^2\chi(k)$ and $k^3\chi(k)$ functions, according to the procedure described in Ref. 23. Nevertheless, S_0^2 was also treated as a free parameter in the fit, whenever it was possible, in order to check its overall agreement with predicted values and its influence on the (most correlated) parameters σ_{ij}^2 and N_j. The reported E_0 values were checked using the procedure similar to the one for the S_0^2 estimation, i.e. through observing $R_i(E_0)$ dependencies for $k\chi(k)$, $k^2\chi(k)$ and $k^3\chi(k)$. The quality of a particular fit was evaluated by using the reduced chi-square method (χ_ν^2), as implemented in FEFFIT program, and the corresponding fit-quality factor R is reported for all presented fits. The significant digit and uncertainty are also provided by FEFFIT, and reported along with the fitted values.

RESULTS AND DISCUSSION

Te K-edge at RT

$Pb_{0.998}Mn_{0.002}Te$ (sample 1)

In the analyses of the $Pb_{1-x}Mn_xTe$ system we started from the simplest case, resolving the structure of the first coordination around Te in the sample with the lowest Mn concentration. Due to very low Mn concentration, the impurity introduced effects can be noticed only indirectly through their influence on overall lattice parameters. The following models are considered for the first coordination structure around Te:

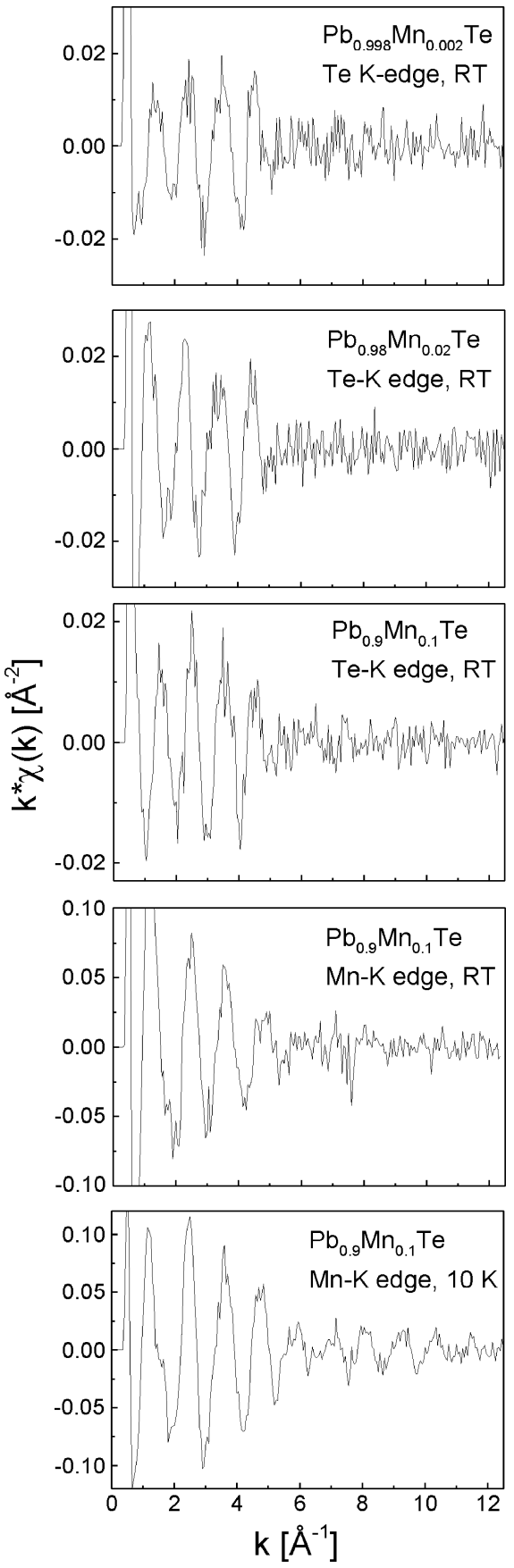

Figure 3. $\chi(k)$ spectra, as extracted from the $\mu(E)$ for some characteristic cases. Each $\chi(k)$ function is multiplied by k to emphasize the high-energy oscillations.

Copyright © 2007 John Wiley & Sons, Ltd.

DOI: 10.1002/xrs

- Single, homogenous Pb shell.
- Single Pb shell with vacancies.
- Two Pb sub-shells.

The results of the model with two Pb sub-shells are presented in Table 1 (first entry). The experimental data and the fit (dashed line) obtained according to this model are presented in Fig. 4(a). The fit is of an acceptable quality and the more abundant shell of Pb atoms is found at the position which is, in the limit of error, identical to the one obtained by XRD[14] (Table 1). The relatively (in the framework of the investigated systems) small value of parameter σ_{Pb}^2, indicates that this Pb shell is well defined. Fit also predicts that a very small amount of Pb atoms (much smaller than one atom per first shell) could be at a substantially larger distance than the regular Pb shell, but not so large as to be considered a vacant site.

The structural models considered in the simultaneous fit of the first and the second coordination were:

- Single homogenous first Pb shell and single homogenous second Te shell.
- First coordination with two Pb sub-shells and second with single Te shell.
- Single Pb shell in the first coordination, and Te coordination divided into two sub-shells.
- First coordination consisting of two Pb sub-shells and second of two Te sub-shells.

The experimental data and the fit corresponding to the last of the models considered (Table 1 second entry) are presented in Fig. 4(b). The value obtained for the more abundant of the Te–Te distances is slightly lower, though in the limit of error equal to the XRD value.[14] The other Te–Te distance is considerably longer. The second coordination σ_{Te}^2 value is significantly larger than the first shell one (σ_{Pb}^2). From Fig. 4(b), it is obvious that some additional parameters should be included to describe all the details of the observed structure. We tried to improve the fit of the second coordination using different combinations of sub-shells and vacancies, considering in some cases the influence of the third shell also. The analyses revealed that the information content in the measured spectra is not enough for the exact characterization of all the details of the second coordination, though it is evident that the Te sub lattice introduces substantional disorder in the structure. The existence of the vacant Te positions in the second coordination is very probable, but their exact number could not be precisely determined at this stage of investigations.

$Pb_{0.98}Mn_{0.02}Te$ (sample 2)

In addition to the models investigated for Sample 1, here, we have also included the possibility that Mn can be found in the coordination together with Pb. The results of the two most reliable fits are presented in Table 1. The experimental data and the fit (dashed line) of the first coordination around Te with two Pb shells, is presented in Fig. 4(c). This model evidently provides the best result among the investigated models for the first coordination of this sample. The higher σ_{Pb}^2 values than those obtained for Sample 1 (see Table 1) point out the larger configurational disorder in the first shell of Sample 2. Two possibilities for the first coordination structure have been obtained. The first one, with two Pb sub-shells with approximately the same number of Pb atoms in each at distances quite close to each other, is, actually, a different expression of the large disorder of the shell, described through the large σ_{Pb}^2 value in the initial fit with only one Pb shell. The other possibility, similar to Sample 1, assumes the existence of a very small concentration of Pb atoms at the well-defined and considerably longer distance than that of the regular shell Pb atoms. As in Sample 1, it appears that existence of vacancies is not probable at the Pb lattice sites of Sample 2. Introduction of Mn in the fitting of the first coordination has not provided any improvement. This result is expected since the Mn concentration in this

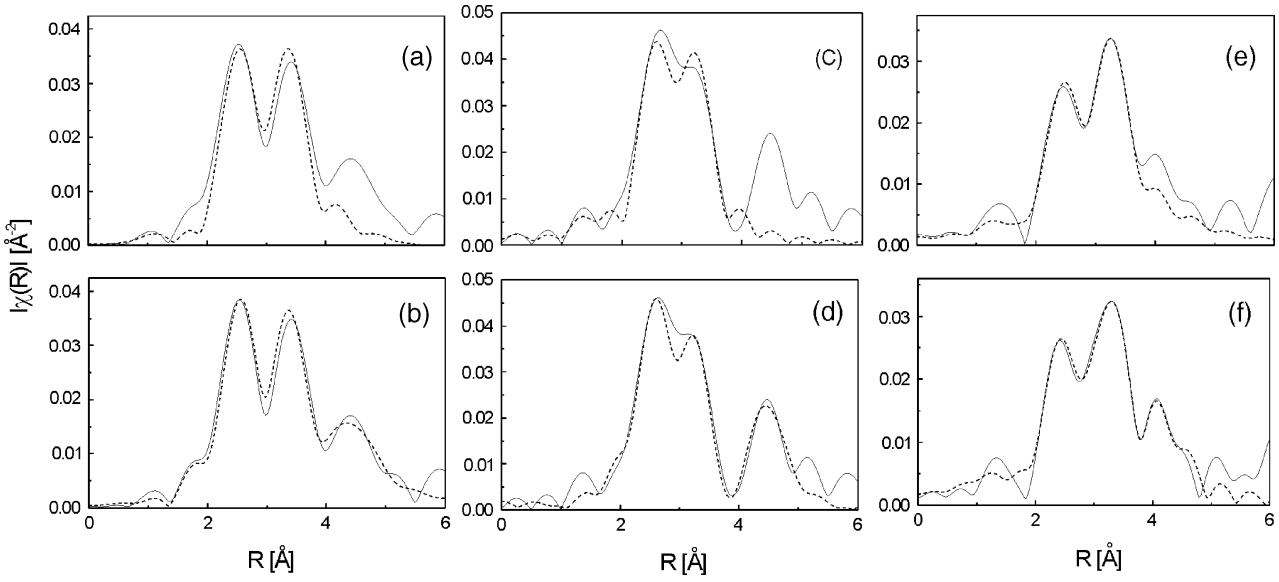

Figure 4. Experimental EXAFS spectra obtained from the Te K-edge at RT, and fit (dashed line) in R-space of the first coordination and the first and the second coordination together, of Sample 1 ($Pb_{0.998}Mn_{0.002}Te$) (a) and (b), Sample 2 ($Pb_{0.98}Mn_{0.02}Te$) (c) and (d), Sample 3 ($Pb_{0.9}Mn_{0.1}Te$) (e) and (f), respectively.

Copyright © 2007 John Wiley & Sons, Ltd.

DOI: 10.1002/xrs

X-RAY Spectrometry

Table 1. Parameters obtained by fitting the Te K-edge EXAFS spectra of Samples 1 ($Pb_{0.998}Mn_{0.002}Te$), 2 ($Pb_{0.98}Mn_{0.02}Te$) and 3 ($Pb_{0.9}Mn_{0.01}Te$) at RT. Table entries are given in the following order: (1) two Pb sub-shells in the 1st coordination; (2) two Pb sub-shells in the 1st and two Te sub-shells in the 2nd coordination. Values without an explicit error are derived from the appropriate fitted values; fixed values are marked with asterisk

Sample	$Pb_{0.998}Mn_{0.002}Te$ $S_0^2 = 0.9$				$Pb_{0.98}Mn_{0.02}Te$ $S_0^2 = 0.9$				$Pb_{0.9}Mn_{0.1}Te$ $S_0^2 = 0.9$			
	First coordination		Second coordination		First coordination		Second coordination		First coordination		Second coordination	
Parameter	Te–Pb_1	Te–Pb_2	Te–Te_1	Te–Te_2	Te–Pb_1	Te–Pb_2	Te–Te_1	Te–Te_2	Te–Pb_1	Te–Mn	Te–Te_1	Te–Te_2
r_{XRD} [Å]	3.230		4.568		3.225		4.561		3.215		4.547	
r[Å]$^{(1)}_{(2)}$	3.23(2)	3.97(9)	—	—	3.19(4)	3.94(4)	—	—	3.22(2)	3.44(3)	—	—
σ^2	3.24(2)	4.00(7)	4.58(5)	4.88(4)	3.21(3)	3.95(5)	4.43(5)	4.6(1)	3.23(3)	3.46(3)	4.62(4)	4.8(1)
Σ^2	0.010(3)	0.01*	—	—	0.013(2)	0.013*	—	—	0.015(2)	0.015*	—	—
	0.011(2)	0.011*	0.016(5)	0.016*	0.014(3)	0.01(1)	0.010(5)	0.010*	0.016(3)	0.016*	0.06(4)	0.06*
E_0	7(1)	7*	—	—	4(1)	4*	—	—	5.6(8)	5.6*	—	—
	6.4(9)	6.4*	6(2)	6*	3(1)	3*	5(2)	5*	5(1)	5*	3(2)	3*
n	5.6(3)	0.4	—	—	5.3(3)	0.7	—	—	5.7(1)	0.3	—	
	5.6(2)	0.4	10.3(9)	1.7	5.4(5)	0.6	6(2)	6	5.8(1)	0.2	9.3(7)	2.7
R	0.019				0.019				0.022			
	0.011				0.017				0.017			

S_0^2, amplitude correction; r, interatomic distance; σ^2, Debye–Waller factor along a bond direction; E_0, phase-shift correction; n, number of atoms included in fitting; R, goodness of fit.

sample is still too low to be observed directly in the first coordination around Te.

The experimental data and the fit (dashed line) of the first coordination consisting of two Pb shells and the second coordination consisting of two Te sub-shells, is presented in Fig. 4(d). First shell parameters are consistent with the results obtained by fitting the first coordination alone, giving confidence in their reliability. The fit provide about 0.1 Å shorter distance for the more abundant second coordination than the XRD measurements, and the pretty large σ_{Te}^2 value. The experimental spectra indicate the very complex structure of the second coordination. We have examined various possibilities as presented in Table 1; we believe that the results are the most reliable. As in Sample 1, it was not possible to form a decisive conclusion about all the details of the second coordination structure from these data alone. There are some indications that Te atoms might be distributed in several sub-shells, or even randomly in the pretty large interval of distances around the mean value provided approximately by XRD and our fit. The existence of vacant positions in this coordination is also highly probable. As could be expected,[23] the inclusion of the third coordination stabilizes parameters of the second coordination in the fitting procedure, but of course, no reliable parameters of the third coordination can be obtained from the measured spectra. For a definite conclusion about the second coordination structure, the multiple fitting procedures of the data obtained at different absorption edges and temperatures are necessary.

$Pb_{0.9}Mn_{0.1}Te$ (sample 3)

Similar structural models as for the previous samples were examined, and the most reliable results are presented in Table 1. The experimental data and the fit (dashed line) of the first coordination shell around Te are presented in Fig. 4(e). Introduction of the Mn sub-shell was necessary for reliable fit of the Te first coordination. The Mn concentration found, roughly corresponds to the one predicted by stoichiometry. The experimental data and the fit (dashed line) of the first and the second coordination fitted together are presented in Fig. 4(f). The first coordination was fitted by one Pb and one Mn sub-shell, and the second coordination by two Te sub-shells. After the introduction of the second coordination, corresponding parameters of the first coordination remain stable, which proves their reliability. The fit provides reasonable results of the principle parameters, with distances of the more abundant shells in both coordinations in good accordance with XRD data. Similar to the Samples 1 and 2, all the details of the two coordinations could not be uniquely described by the fitting procedure used. The exact structure of the second shell of this sample is also in question, but it is evident that its contribution is clearly weaker than in Samples 1 and 2, implying a larger disorder or (and) more vacancies in the Te second coordination of Sample 3, than it has been observed in Samples 1 and 2.

Mn K-edge of sample 3 ($Pb_{0.9}Mn_{0.1}Te$)

RT

In the analyses of these experimental data, we have followed the idea that Mn, in general, enters the lattice positions by replacing Pb, so that overall lattice structure remains in average of the NaCl type, as provided by XRD measurements presented in Fig. 1. Nevertheless, special attention is paid to determination of the exact local structure around Mn atoms, because there are a lot of indications (difference between Mn and Pb ion radii and polarisabilities, different (NiAs) structure of MnTe, previous measurements[13,14]) that it could be significantly different from that of Pb. On that

Copyright © 2007 John Wiley & Sons, Ltd.

DOI: 10.1002/xrs

Table 2. Parameters obtained by fitting the Mn K-edge EXAFS spectra of Sample 3, ($Pb_{0.9}Mn_{0.1}Te$) at RT and at 10 K. Table entries referring to NaCl structure constrains are given in the following order: (1) two Te sub-shells in the 1st coordination; (2) two Te sub-shells in the 1st and, one Pb sub-shell and one Mn sub-shell in the 2nd coordination. Table entries referring to NiAs structure constrains are given for the single Te shell in the first coordination. Values without an explicit error are derived from the appropriate fitted values; fixed values are marked with asterisk

Sample	$Pb_{0.9}Mn_{0.1}Te$ (RT) $S_0^2 = 0.7$					$Pb_{0.9}Mn_{0.1}Te$ (10 K) $S_0^2 = 0.9$				
	First coordination (NaCl)		First coordination (NiAs)	Second coordination (NaCl)		First coordination (NaCl)		First coordination (NiAs)	Second coordination (NaCl)	
Parameter	Mn–Te_1	Mn–Te_2	Mn–Te	Mn–Pb	Mn–Mn	Mn–Te_1	Mn–Te_2	Mn–Te	Mn–Pb	Mn–Mn
r[Å][1]	3.50(4)	2.71(9)	2.90(2)	—	—	3.465(3)	2.785(9)	2.869(9)	—	—
[Å](2)	3.50(2)	2.66(5)		4.48(4)	4.65(3)	3.464(3)	2.78(1)		4.62(1)	4.51(6)
σ^2	0.006(6)	0.006*	0.007(3)	—	—	0.0026(4)	0.0026*	0.003(1)	—	—
	0.006(3)	0.006*		0.009(3)	0.012(7)	0.0030(3)	0.0030*		0.005(1)	0.005*
E_0	−2(2)	−2*	−0.6(7)	—	—	−1.3(2)	1.3*	0.3(7)	—	—
	−1.9(9)	−1.9*		0(2)	0*	−1.2 (2)	−1.2*		−2(1)	4(3)
n	3.5(9)	2.5	4.2(6)	—	—	4.2(1)	1.8	5.1(6)	—	—
	3.4(7)	2.6		5(2)	7	4.5(2)	1.5		6.6(8)	5.4
R	0.049		0.033	0.049		0.0027		0.024	0.0027	
	0.054			0.054		0.0022			0.0022	

S_0^2, amplitude correction; r, interatomic distance; σ^2, Debye–Waller factor along a bond direction; E_0, phase-shift correction; n, number of atoms included in fitting; R, goodness of fit.

course, we have also examined the possibility that Mn can be incorporated in the host NaCl lattice in the way that its immediate surrounding i.e. the first coordination formed of Te atoms is more like that in hcp MnTe than in fcc NaCl PbTe structure. The best fit results of these two different models are presented in Table 2. It turned out that, as long as the first coordination is considered, both models give reasonable results, suggesting that Mn tends to keep its immediate surrounding as close to the one in the NiAs structure, as the host structure allows, deforming it appreciably.

The procedure described in Section Samples, EXAFS Measurements and Data Processing for determination of S_0^2 provided a value of $S_0^2 = 0.7$, which was used in subsequent analyses. The self-absorption at Mn edge turned out to be negligible. Introducing two Te sub-shells under NaCl structural constraints in the fit of the first Mn coordination (Fig. 5(a)), provided the results presented in Table 2. The more abundant (approximately four atoms) Te sub-shell is at the same distance as the Mn atoms in the first coordination of Te, as obtained from the Te K-edge fit (Table 1.), but with much smaller σ^2 value. The second Te sub-shell is at a considerably shorter distance. This leads to a conclusion that the local structure around Mn in this sample at RT substantially deviates from that predicted by XRD measurements. The reason could be the significant off-centering of Mn ions from the regular lattice positions or(and) large disorder in the Te sublattice, already observed in the analyses of Te K-edge data (Table 1), which includes both deviations of the distances and existence of vacancies. The best fit of the first coordination with homogenous Te shell, under the NiAs structural constraints is presented in Fig. 5(b), and the corresponding results are given in Table 2. So obtained value of the Mn–Te distance agrees well with the one in the MnTe lattice.[11]

The best fit of the first (represented by the two Te sub-shells) and the second (represented by a Pb sub-shell and a Mn sub-shell) coordination together is presented in Fig. 5(c), and the corresponding results are given in Table 2.

T = 10 K

In order to investigate the Mn behavior in the PbTe lattice in more details we performed measurements at 10 K, the temperature below the suspected phase transition[13,14] related to eventual Mn off-centering, FPT and even magnetic reordering of Mn ions. These data allow much better resolution of the structural parameters than the RT ones. Similar to the analyses of the Mn K-edge data at RT, the fit of the first Mn coordination with the homogenous Te-shell have not provided satisfactory results. The fit of the first Mn coordination with the two Te sub-shells under the NaCl structural constrains, is presented in Fig. 5(d). The results are similar to the corresponding results obtained at the same edge at RT, but much more reliable. The more abundant Te sub-shell (consisting of four atoms) is at the distance which is longer than the Te–Pb distance in any of the measured samples and also longer than the mean value obtained by the presented and XRD measurements in Ref. 14 The second Te sub-shell (consisting of two atoms) is at a much shorter distance than the first one, and much shorter than the corresponding Pb–Te one. According to small σ^2 values, both Te sub-shells are very well defined. The results obtained for the first shell under NiAs structural constrains

Copyright © 2007 John Wiley & Sons, Ltd.

DOI: 10.1002/xrs

X-RAY Spectrometry

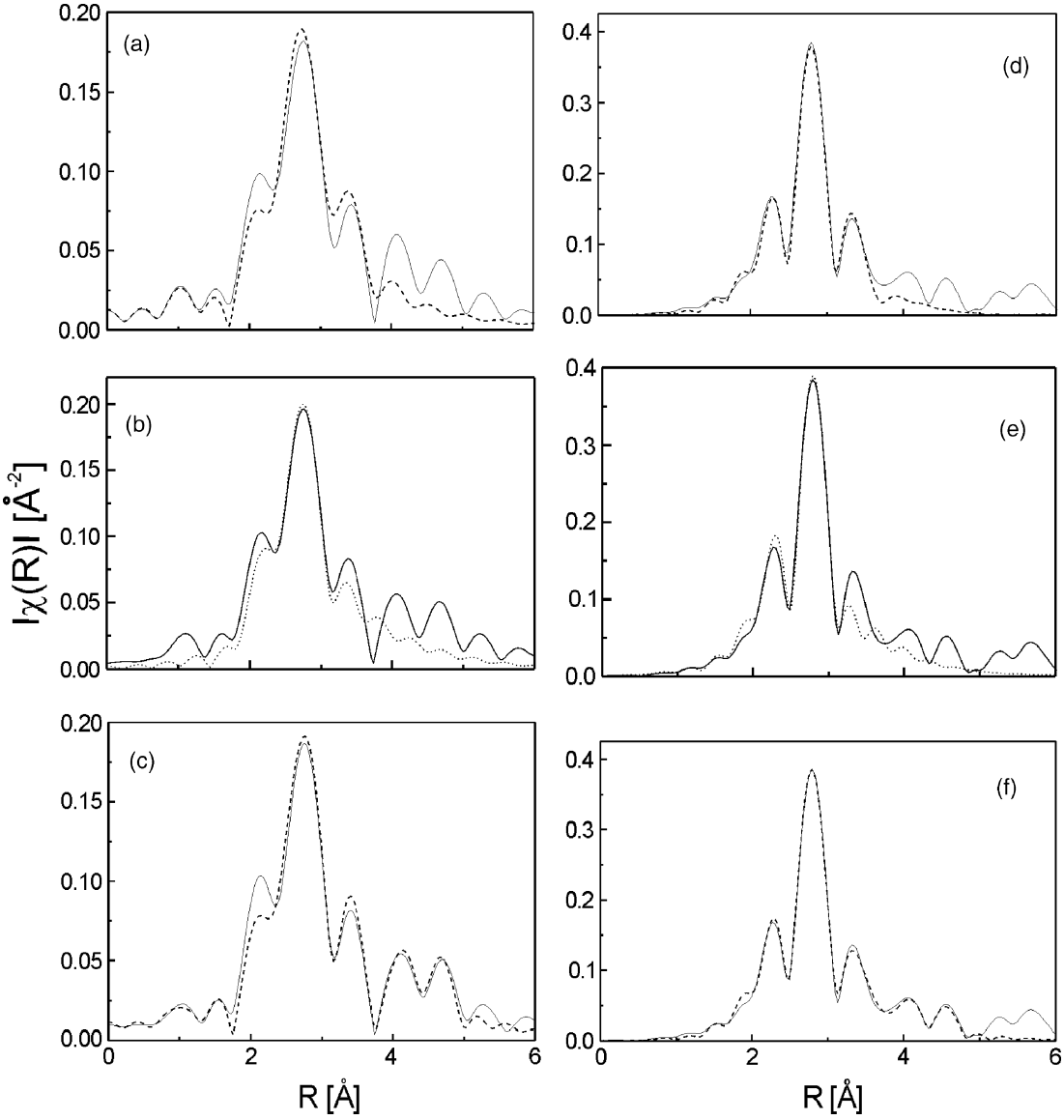

Figure 5. Experimental EXAFS spectra obtained from the Mn K-edge, and fit (dashed line) in R-space of (a) the first coordination (b) the first coordination under NiAs structure constrains (c) the first and the second coordination at RT, (d) the first coordination (e) the first coordination under NiAs structure constrains (f) the first and the second coordination at 10 K, of Sample 3 ($Pb_{0.9}Mn_{0.1}Te$).

(Fig. 5) again provide results very close to the ones that should be expected for the pure MnTe structure (Table 2).

The best fit of the first (two Te sub-shells) and the second (a Pb sub-shell and a Mn sub-shell) coordination together is presented in Fig. 5(f).

The fit is of very good quality, with well-defined parameters. Parameters of the first shell remain stable after the second shell inclusion. The distance of the Pb sub-shell in the second coordination is longer and that of the Mn sub-shell is shorter than the mean value predicted by XRD measurements.[14] This suggests that despite the fact that most of the Mn–Te bonds in the first coordination are longer than Pb–Te distance, Mn atoms tend to stay in the structure as close as possible to each other, producing some very short Mn–Te bonds, to enable this. In addition, there are clearly more Mn atoms in the second Mn coordinations than it is predicted by the stoichiometry. Both of these facts strongly allude on the situation present in MnTe, where two Mn atoms in the second coordination of Mn, are very close to the referent one.

CONCLUSIONS

We investigated $Pb_{1-x}Mn_xTe$ samples with different Mn concentration ($x = 0.002, 0.02, 0.1$) using EXAFS measurements at Te K-edge at RT and Mn K-edge at RT and 10 K. Intrinsically, the systems are of the NaCl structure type, with Mn ions replacing Pb in the unit cell. As it has been found previously in similar systems, the compounds are quite disordered at RT, and disorder increases with the increase of Mn concentration. The distance of the Pb atoms in the first coordination around Te is well defined, in the limit of the experimental error identical to the one predicted by XRD, and does not deviate much with the Mn content. It suggests the importance and stability of the particular bond types in such multicomponent systems. The effect of disordering of

Copyright © 2007 John Wiley & Sons, Ltd.

DOI: 10.1002/xrs

the structure with increase of Mn-concentration is manifested in the Pb shell in two aspects:

(1) Through the increase of the mean square displacement along the Te–Pb bond direction σ^2 (see Tables), which is considerably smaller for the $x = 0.002$, than for the $x = 0.02$ and 0.1 samples, being approximately the same for the last two samples.
(2) Through the possible displacement of the small number (one in every third or fourth immediate Te coordination) of Pb atoms at the well-defined distance considerably longer than the average for the Pb-Te. In the $x = 0.1$ sample, approximately the same amount of Mn in the first coordination around Te has been found instead of these Pb atoms, at the distance between the two Pb's.

The second (Te) coordination around Te is more poorly defined than the first one, being progressively worse as x increases. One of the reasons could be a significant amount of vacancies, that are known to exist in these systems. The number of vacancies in the second shell rises with x, resulting in a progressively lower number of the second shell Te atoms contribution to the EXAFS signal. The Te–Te distance close to the corresponding XRD value is possible to obtain only if the second Te sub-shell is included, or the third coordination contribution to the second one is taken into account. Generally, a large influence of the third on the second coordination has been noticed in all the samples, as another indication of the high intrinsic disorder of the samples. Due to this disorder, we were able to resolve only the major parameters, but not all the details of the second coordinations structure at RT, either from the Te K-edge, or from the Mn-edge, in any of the investigated samples. We hope to overcome this problem by using multiple data sets fitting procedures, and if necessary, after conducting some additional measurements.

The Mn–Te distances obtained from the two different edges at RT are in a good agreement. Under the NaCl structural constraints, the majority of the Mn–Te distances are longer than the Pb–Te ones, which is in contradiction to the stronger Mn–Te than Pb–Te bonding expected from their phase system analyses and smaller Mn than Pb ion size. However, the rest of the Mn–Te bonds are very short, particularly at 10 K. The σ^2 values of these bonds are much smaller than those of the Pb–Te bonds, both for the atoms in the first and in the second coordination, indicating that the local structure around Mn is, in that sense, better defined. The existence of two extremely different Mn–Te distances and less Mn atoms around Te (looking from the Te edge) than stoichiometry predictions, indicate the off-centering of the Mn atoms from the regular lattice positions. Also, there are undoubtly more Mn atoms in the second shell around Mn than stoichiometry predictions, especially at 10 K, suggesting some kind of preferential occupation of the lattice sites by Mn atoms, placing them much closer to each other than the random distribution predictions. However, this is not really clustering, since Mn atoms are not in each other's immediate coordinations. Very good fit obtained for the first shell around Mn using NiAs structural constrains suggest that, to the extent allowed by the host lattice, Mn tends to coordinate itself as in MnTe. This finding explains the deviations from the NaCl structure noticed around Mn.

The results of our preliminary calculations using WIEN2k package[26] indicate that introduction of Mn highly influences density of states in the region of the energy gap, pushing the Fermi level to the bottom of the conduction band and fixing it to Mn-d states. We expect that these calculations and XANES analyses of our experimental data, which are in progress, will relate the electronic structure of the compounds and interesting structural features presented in this work.

Acknowledgement

The authors from Belgrade are grateful to the Serbian Ministry of Science and Environmental protection for the financial support of this work.

REFERENCES

1. Volkov BA, Ryabova LI, Khokhlov DR. *Usp. Fiz. Nauk. Rusian Acad. Sci.* 2002; **172**: 875. [Engl. Trans. Physics—Uspekhi. 2002; 45: 819–846].
2. Yang Y, Li W, Yu L, Sun X, Xu L, Hou L. *Infrared Phys. Technol.* 1997; **38**: 9.
3. Dresselhaus MS, Dresselhaus G, Sun X, Zhang Z, Cronin SB, Koda T, Ying JY. *Microscale Thermophys. Eng.* 1999; **3**: 89.
4. Lebedev AI, Sluchinskaya IA, Demin VN, Munro IH. *Pis'ma Zh. Eksp. Teor. Fiz.* 1996; **63**: 600, [Engl. *Trans. JETP Letters.* 1996; 63: 635–667.
5. Wang Z, Bunker BA. *Phys. Rev., B* 1992; **46**: 11277.
6. Lebedev AI, Sluchinskaya IA, Demin VN, Munro IH. *Phys. Rev., B* 1997; **55**: 14770.
7. Ravel B, Cockayne E, Newville M, Rabe KM. *Phys. Rev., B* 1999; **60**: 14632.
8. Kavamura H. In *Proceedings Third International Conference Physics Narrow-gap Semiconductors*, Warsaw, 1977; 7.
9. Katayama S, Murase K. *Solid State Commun.* 1980; **36**: 707.
10. Islam QT, Bunker BA. *Phys. Rev. Lett.* 1987; **59**: 2701.
11. David R. Lide (ed). *CRC Handbook of Chemistry and Physics, 1st Student edition*. CRC Press: Boca Raton, FL, 1988.
12. Tessman JR, Kahn AH, Schockley W. *Phys. Rev.* 1953; **92**: 890.
13. Tholence J, Mauger A, Escorne M, Triboulet R. *J. Appl. Phys.* 1984; **55**: 2313.
14. Romčević N, Golubović A, Romčević M, Trajić J, Nikolić S, Durić S, Nikiforov VN. *J. Alloys Compd.* 2005; **402**: 36.
15. Mikkelsen JC, Boyce JB. *Phys. Rev., B* 1983; **28**: 7130.
16. Balzarotti A, Motta N, Kisiel A, Zimnal-Staranawska M, Czyzyk MT, Podgorny M. *Phys. Rev., B* 1985; **31**: 7526.
17. Pong W-F, Mayanovic A, Bunker BA, Furdyna JK, Debska U. *Phys. Rev., B* 1990; **41**: 8440.
18. Newville M. *J. Synchrotron Radiat.* 2001; **8**: 322.
19. Ankudinov AL, Ravel B, Rehr JJ, Conradson SD. *Phys. Rev., B* 1998; **58**: 7565.
20. Newville M, Lıviņš P, Yacoby Y, Rehr JJ, Stern EA. *Phys. Rev., B* 1993; **47**: 14126.
21. Ravel B. *J. Synchrotron Radiat.* 2001; **8**(2): 314.
22. Stern EA, Newville M, Ravel B, Yacoby Y, Haskel D. *Physica B* 1995; **208&209**: 117.
23. Ravel B. *EXAFS Analysis with FEFF and FEFFIT*, http://feff.phys.washington.edu/~ravel/. [12 April 2001].
24. Ravel B, Newville M. *J. Synchrotron Radiat.* 2005; **12**: 537.
25. Koningsberger DC, Prins R. *X-Ray Absorption-principles, Applications, Techniques of EXAFS, SEXAFS and XANES*. John Wiley and Sons: Chichester, 1987.
26. Blaha P, Schwarz K, Madsen GKH, Kvasnicka D, Luitz J. WIEN2k, *An Augmented Plane Wave+Local Orbitals Program for Calculating Crystal Properties*. K. Schwarz, Techn. Universtät: Wien, 2001; ISBN 3-9501031-1-2.

Copyright © 2007 John Wiley & Sons, Ltd.